Short Crack Initiation and Growth at 600°C in Notched Specimens of Inconel718

T. Connolley, P. A. S. Reed, M. J. Starink
Materials Research Group, School of Engineering Sciences
University of Southampton, Highfield, Southampton, SO17 1BJ, United Kingdom

Keywords: crack initiation, Ni superalloys, carbide, oxidation

ABSTRACT

The natural initiation and growth of short cracks in Inconel® 718 U-notch specimens has been studied at 600°C in air. U notches were introduced through broaching, and hardness traces and optical microscopy on cross sections through the U notch broaching showed that the broaching process had introduced a deformed, work hardened layer. Fatigue tests were conducted under load control using a 1-1-1-1 trapezoidal waveform, on specimens with as-broached and polished U-notches. Multi-site crack initiation occurred in the notch root. Many of the cracks initiated at bulge-like features formed by volume expansion of oxidising (Nb,Ti)C particles. In unstressed samples, oxidation of (Nb,Ti)C particles occurred readily, producing characteristic surface eruptions. Scanning electron microscopy on metallographic sections revealed some sub-surface (Nb,Ti)C oxidation and localised matrix deformation around oxidised particles. A mechanism for crack initiation by carbide expansion during oxidation is discussed. Surface short crack growth rates in the notch root of polished specimens were measured using an acetate replica technique. Observed short crack growth rates were approximately constant across a wide range of crack lengths. However, there was a transition to rapid, accelerating crack growth once cracks reached several hundred microns in length. This rapid propagation in the latter stages of the fatigue life was assisted by crack coalescence. Polishing the U-notch to remove broaching marks resulted in a pronounced increase in fatigue life.

1. Introduction

Nickel-base superalloys like Inconel®718 (IN718) are used extensively for turbine discs and other components in industrial and aerospace gas turbines. Since turbine discs are safety-critical components, considerable effort is expended in determining their safe operating life. The lifing procedure adopted must enable the reliable prediction of the safe life of the disc, without being overly conservative. Once engines are in service, regular inspection of the engines and refinements of lifing models may enable life-extension programs to be considered. In the traditional predicted safe life philosophy, the life is declared based on laboratory specimen and component testing. In recent years a damage-tolerant approach to lifing has been adopted, in which it is accepted that components contain defects or inhomogeneities from which cracks can initiate. Assuming an initial flaw size c_o, the fatigue life is determined as the number of cycles required to propagate the crack to some critical size c_c. The initial size c_o can be based on the maximum defect size present in the material, or on the minimum defect size detectable by non-destructive testing (NDT) [1]. Selection of c_c is based on knowledge of the fracture toughness of the material, the limit load, the maximum allowable strain or maximum permitted compliance change for a particular component. Damage-tolerant lifing requires accurate information on fatigue crack initiation and growth rates. Fatigue lives are determined by integration of equations relating the crack growth rate to a characteristic driving force, such as the elastic stress intensity

factor range ΔK, or the J-integral range ΔJ. Interest in retirement-for-cause of discs and life extension programmes highlights the need for further understanding of the damage processes that can occur in service.

One type of in-service damage to turbine discs is low cycle fatigue (LCF) cracking in the fir tree root fixtures. These are notch-like features (see Fig. 1), so lifing of the disc must consider the behaviour of cracks in notched members. This is more complicated than for cracks in plain specimens because of the stress concentrating effect of the notch, which may be sufficient to cause yielding of the material in the notch root. A complete picture of crack propagation behaviour in a turbine disc must also consider the differences in behaviour between short cracks and long cracks [2]. Just after initiation, a crack may be small relative to the grain size of the material. Interactions between the growing crack and grain boundaries may result in crack arrest, retardation or deflection. In a notch root, the crack may be mechanically short relative to the size of the notch plastic zone. This may result in retardation or arrest of a short crack due to plasticity-induced closure. However, closure of short cracks is limited due to their short wake and short cracks can have faster growth rates than long cracks subjected to the same nominal crack driving force ΔK. In the past, this has led to non-conservative estimates of fatigue lives when long crack data alone has been used [1, 3]. Short cracks can also grow at ΔK levels below the threshold stress intensity range (ΔK_{th}) determined for long cracks.

The present study is performed on Inconel® 718 (IN718) superalloy, which is a nickel-base precipitation strengthened alloy widely used in gas turbine designs. For example, IN718 represents 34% by weight of the materials used in the General Electric CF6 turbofan engine [4]. A considerable amount of work has been performed to characterise the effect of temperature and environment on long crack propagation rates in IN718. For temperatures up to 650°C, it was found that the main time-dependent process influencing fatigue crack propagation was grain boundary oxidation [5, 6, 7]. Hold times at maximum or minimum load in the fatigue cycle were found to significantly increase crack growth rates, with the dwell allowing time for oxide embrittlement of grain boundaries to occur [8-14]. Most of these studies were on long cracks using CT specimens, but the hold time effect has also been observed for pre-initiated cracks in U-notch specimens tested in bending [15].

Although the high temperature growth rates of long cracks in IN718 have been extensively characterised, relatively little is known about high temperature crack initiation and short crack growth, particularly in notched geometries like a turbine disc rim. Partly this is due to the experimental difficulties of observing short cracks at high temperature. For a variety of superalloys, high temperature crack initiation has been observed at slip bands [16, 17], inclusions [18], pre-cracked carbide particles [19] and preferentially oxidised carbides [20-23]. In some superalloys, primary carbides have script-like morphologies, which react to form oxide intrusions from which fatigue cracks can grow. However, in wrought IN718, primary carbides usually have a globular morphology and the mechanism by which carbide oxidation affects fatigue behaviour may be different. In a study of notch-rupture sensitivity of IN718 [24], volume expansion of oxidising primary carbides was identified as a mechanism of environmentally assisted crack propagation, due to the stress intensifying effect of expanding particles at or near crack tips. Surface eruptions of oxidised material in IN718 have been observed [24, 25], and evidence of fatigue crack initiation at oxidised carbides in IN718 has recently been reported [26, 27].

The purpose of the research presented in this paper was to study the natural initiation, growth and interaction of short cracks in notched IN718 specimens at 600°C in air. These conditions are similar to those experienced in the fir tree root fixings of a gas turbine disc. Study of initiation and short crack growth behaviour under conditions similar to those experienced in service will aid understanding of phenomena observed in actual components. For example, a study on retired IN718 turbine discs showed that cracks in slot bottoms appeared early on in the component life, but took a long time to grow [28]. The paper covers in more detail the reported evidence of fatigue crack initiation at oxidised carbides [26, 27], and discusses the observed short fatigue crack propagation and interaction behaviour.

2. Experimental Procedure

2.1. Material

Material used in this study was taken from a heat treated Inconel 718 turbine disc forging. The forging was solution treated at 955°C for 1 h followed by an air cool. It was then aged at 720°C for 8 h, cooled at 50K/h to 620°C, then aged at 650°C for a further 8 h, finishing with an air cool. The composition in wt. % is given in Table 1.

2.2. Metallography and microscopy

Metallographic specimens of the as-received material were prepared and examined in the as-polished and etched conditions. The etchant used was Nimonic etch (10 ml HNO_3, 50 ml HCl, 40 ml H_2O & 2.5g $CuCl_2$). Optical microscopy combined with image analysis was used to determine grain size and the primary carbide volume fraction. For fractography and further metallography a JEOL JSM 6400 scanning electron microscope (SEM) was used. To confirm the identity of phases present, energy-dispersive X-ray spectrometer (EDS) was employed.

2.3. Low cycle fatigue testing

Fatigue testing was performed on single-edged U-notch bend specimens. The specimen geometry is shown in Fig. 2. The theoretical elastic stress concentration factor was calculated by an elastic finite element model to be 2.08. Specimens were extracted from locations close to the rim of the disc forging, as shown in Fig. 3. The longitudinal axes of the specimens were tangential to the disc circumference, and the notch axis in each specimen was parallel to the disc axis. Notches were machined using a broaching process similar to that used for machining fir tree root fixings in production discs. The broaching process produced long machining marks parallel to the notch axis. Notch surface roughness measurements were made using a Talysurf instrument. The average R_a value obtained was 0.16 μm and the maximum valley depth R_v detected was 2.16 μm. Metallography was performed on cross-sections through the notches of selected specimens to check for any microstructural changes arising from the broaching process.

Fatigue testing was conducted at 600°C inside a high temperature chamber mounted on an Instron 8501 servo-hydraulic testing frame. Specimens were heated using four high intensity quartz lamps and the temperature was monitored and controlled to within +/- 2°C via an R-type thermocouple attached to the front face of each specimen. The chamber was equipped with a Balzers turbo-molecular pumping system to enable testing in vacuum. For vacuum testing pressures between 2.5 x 10^{-3} Pa and 3.2 x 10^{-4} Pa were achieved. Tests were conducted in three point bend under load control using a 1-1-1-1 trapezoidal waveform (i.e. the cycle contains subsequent periods at a minimum stress, a linearly rising stress, a maximum stress and linearly

reducing stress, all periods having an identical duration), at a load ratio R = 0.1. For testing purposes, the maximum stress σ_{max} was defined as the net section bending stress in the notch root calculated using simple beam theory. Tests were conducted with σ_{max} = 750 MPa or 790 MPa. For a notch elastic stress concentration factor of 2.08, the peak theoretical elastic stresses were 1560 MPa and 1643 MPa respectively. This is well above the yield stress of IN718 at 600°C, hence in reality the notch root region was plastically deformed by the applied load conditions. Using a proprietary 3-dimensional FEM model, the depth of the plastic zone was estimated to be 0.2mm, using the criterion of equivalent plastic strain $\varepsilon_{pl}^{eq} \geq 0.2\%$.

The majority of testing was conducted in air. Three sets of tests were performed. The first set was performed on specimens with notches in the as-broached condition, to represent the surface finish present in a production turbine disc. These tests were run to failure, then examined in an SEM to identify the crack initiation sites. One specimen was tested in vacuum at σ_{max} = 750 MPa for comparison with the air tests. A second set of tests were performed in air to measure crack growth rates. These tests were interrupted every 2000 cycles in order to take cellulose acetate replicas from the notch root. Replication trials on an as-broached specimen demonstrated that it was extremely difficult to distinguish between cracks and broaching marks in the U-notch. Therefore, the tests were performed with polished notches. The specimens were polished to a 1μm diamond finish. To prevent enlargement of the notch, which can occur during manual polishing, each specimen was clamped in a specially-designed jig and polished using soft cylindrical dental felts 4 mm in diameter and 8mm long mounted in a pillar drill. Crack length measurements from replicas were made with the aid of a calibrated image analysis system connected to the microscope via a high resolution digital camera. Finally, a third set of uninterrupted tests in air were performed on polished specimens.

2.4. Thermal exposure

A series of thermal exposure experiments were performed to study the oxidation of primary carbides in unstressed samples of IN718. Small samples of the disc material were mounted in thermosetting resin so one surface could be polished to 1μm diamond finish. After polishing, the specimens were broken out of the resin, cleaned then thermally exposed in air for 1 – 128 h. Two sets of experiments were performed, one at 550°C and one at 600°C. After thermal exposure, the surfaces of the specimens were examined by SEM and optical microscopy to investigate features produced by oxidation. Selected samples were nickel plated, mounted in conducting thermosetting resin and polished to a 1μm diamond finish, so that the thermally exposed faces could be examined in cross-section.

3. Results

3.1. Microstructure

An SEM backscatter image of the microstructure is shown in Fig. 4. The material had a non-equiaxed grain structure with larger elongated grains (diameter approximately 30-70 μm) surrounded by extensive regions of small, more equiaxed grains (diameter approximately 5-20 μm). The larger grains were elongated in the tangential and radial directions, as would be expected for a forged disc. Grain boundaries were extensively decorated with particles of various morphologies, ranging from globular to almost continuous films. EDS revealed that these particles were the δ (Ni_3Nb) phase. The mean area fraction of primary carbides and nitrides,

determined by image analysis on polished microsections, was 0.37%. It can be shown [29] that the amount of carbides and nitrides is directly determined by C and N content of the alloys, and that the measured volume fraction of carbides and nitrides is consistent with C and N content of the present In718 alloy.

In metallographic sections through the notches of as-broached specimens, a sub-surface layer was observed which had the appearance of a zone of heavy localised deformation (see Fig. 5). This extended all the way round the surface of the U-notch. The thickness of the layer was between 10-16 μm in the notch root and up to 40 μm on the notch sides. Examination of polished specimens showed that the deformation layer was still present after polishing, though its depth in the notch root was reduced to approximately 7-10 μm. Microhardness measurements showed that this deformation layer was approximately 15% harder than bulk material. Tests on other machined surfaces of the same specimens without a visible deformation layer did not exhibit an hardness increase compared to bulk material.

3.2. Primary carbide oxidation

Oxidation of (Nb,Ti)C primary carbides occurred readily in unstressed samples exposed at 550^{o}C and 600^{o}C. Oxidation of the carbides resulted in the formation of characteristic surface eruptions, which were clearly visible using an SEM. On the surfaces polished prior to exposure, the eruptions were often tower-like in appearance when viewed side-on. Examples of such towers are shown in Fig. 6, where the eruptions appear to consist of a series of stacked layers or flakes. Other eruptions on the polished surfaces were more irregular in shape (see Fig. 7). Eruptions were observed on the as-machined faces of specimens too, these eruptions being generally irregular in shape.

Metallographic sections through the thermal exposure specimens enabled observation of the sub-surface oxidation behaviour using optical and scanning electron microscopy. In most cases, only primary carbides which intersected the surface underwent oxidation. The size of carbides observed ranged from 3-17 μm. For short exposure times up to 16 h, some partial oxidation of primary carbides was seen. The depth to which the particles were oxidised increased with increasing exposure times. For exposure times longer than 16 h, complete oxidation of surface-intersecting carbides occurred. Sometimes, localised matrix deformation was observed in the vicinity of the oxidised particles. Occasionally, oxidation of sub-surface primary carbides was observed. Bulges in the matrix could be seen above the oxidised particles, an example of which is shown in Fig. 8.

3.3. Crack initiation in U-notch specimens

Crack initiation sites in as-broached specimens were studied by post-fracture examination in an SEM. In all tests, multi-site crack initiation occurred in the notch root. In air, three main types of crack initiation site in air were identified:

(i) Surface eruptions formed by the oxidation of primary carbides (see Fig. 9)
(ii) Bulge-like features associated with the oxidation of sub-surface primary carbides (see Fig. 10 to Fig. 13).
(iii) Sites with no surface eruption or bulge.

In vacuum, primary carbide oxidation was suppressed. Surface eruptions were absent and no crack initiation associated with oxidation of primary carbide particles was observed.

Additional information about the crack initiation process in air was obtained from the interrupted tests on polished specimens. Examination of surface replicas taken during the interrupted tests showed that cracks began to initiate within the first 10% of the overall fatigue life. The evolution of the number of cracks present in the notch root as tests progressed is shown in Fig. 14 for σ_{max} = 750 MPa and σ_{max} = 790 MPa. For both tests, the majority of cracks initiated at bulge-like features, with the remainder starting at surface eruptions or at sites with no discernable eruption or bulge (this will be termed intrinsic initiation). A common feature in both tests was an incubation period at the beginning of the test in which no cracks were observed. After the initial incubation period, the number of cracks increased at a steady rate. The initiation rate then decreased. Eventually, major coalescence of cracks led to rapid reduction in the number of individual cracks observed in the notch root.

3.4. Short crack growth, interaction and coalescence

In this paper, the convention of a crack of surface length 2c is used to describe short crack lengths and growth rates. To allow for the possibility of crack asymmetry, surface cracks are divided into two segments c_1 and c_2. Segment c_1 is the distance from the first crack tip to the middle of the initiation site and c_2 the distance from the second crack tip to the middle of the initiation site, so that $2c = c_1 + c_2$.

Analysis of replicas taken from the roots of polished U-notch specimens showed that many of the cracks which initiated either propagated very slowly or became non-propagating. Significant rates of crack growth were confined to just a few cracks in each specimen and it is the growth rates of these cracks which were studied in detail. However, the other non-propagating or very slowly propagating cracks may have influenced the growth of the propagating cracks due to shielding effects or coalescence. In the later stages of the fatigue life, there was a transition from steady short crack growth to very rapid growth and coalescence of cracks, eventually forming a single crack along the entire notch root which soon resulted in specimen fracture.

Crack length information for the main propagating cracks is presented in Fig. 15. Fig. 15(a) is for a test performed with σ_{max} = 750 MPa and Fig. 15(b) is for a test performed with σ_{max} = 790 MPa. Total crack growth rates d(2c)/dN are plotted against total crack length 2c in Fig. 16. An interesting feature of these short crack growth rates is that there was not a general increase in crack growth rate with increasing crack length, as is normally observed for long cracks. This is particularly noticeable for the test performed at σ_{max} = 750 MPa. Some of the cracks exhibit temporary arrests. Crack I in Fig. 16(a) temporarily arrested at a length 2c = 48 μm. Grain diameters in the IN718 material tested ranged from 5-70 μm, so the temporary arrest of this crack may have been due to the presence of grain boundaries. Other temporary arrests of propagating cracks can be attributed to interactions with other short cracks in the notch root. Referring to Fig. 15(a), segment c_2 of Crack III arrested completely after 28000 cycles, while segment c_1 continued to grow. The arrest of segment c_2 is thought to be due to interaction with the crack tip plastic zone of another crack, as can be seen in Fig. 17. The continued growth of segment c_1 was assisted by coalescence with an adjacent small crack, though the presence of other surrounding cracks may have shielded this crack from the full effects of the applied stress. An absence of shielding, at least in the early stages of propagation, may have contributed to the rapid growth of Crack II in

Fig. 15(a) and Fig. 16(a). However, beyond 28000 cycles, Crack II became asymmetric about its origin, with segment c_1 growing more slowly than c_2. This could be attributed to the shielding effects of other cracks, as shown in Fig. 18.

Substantial coalescence of cracks was confined to the later stages of the fatigue life. In the 750 MPa test, stable short crack growth occurred until the longest crack (Crack II) reached a surface length 2c = 842 μm at 48000 cycles. In the remainder of the fatigue life, rapid growth of this crack occurred, assisted by coalescence with other short cracks in the notch root, resulting in final specimen fracture at 51279 cycles. An example of crack coalescence during the later stages of the fatigue life is shown in Fig. 19.

In the 790 MPa test, the longest crack (Crack A) reached a surface length of 2c = 301 μm at 43000 cycles, beyond which rapid crack growth and coalescence proceeded in the same manner as the 750 MPa test. Final fracture of the specimen occurred at 51687 cycles.

All of the short cracks observed in both specimens were remarkably straight, except where the tips underwent local deflection during crack-crack interactions. This straightness is indicative of transgranular propagation at the surface, supported by fractographic observation of the fracture surfaces. Propagation in the specimen depth direction was initially transgranular, followed by a transition to mixed transgranular-intergranular fracture, as shown in Fig. 20. Mixed transgranular-intergranular propagation was observed on all specimens tested in air, but for the test conducted in vacuum the propagation mode was transgranular.

In order to characterise short crack growth, nominal ΔK values were calculated for the short cracks in the U-notches. This allows comparison with long crack data [30] obtained for similar IN718 material tested under the same conditions. Comparison on the basis of ΔK is a standard method of characterising short crack growth behaviour, despite the clearly elasto-plastic conditions invalidating K as a reliable description of the short crack tip stress and strain field. The cracks in the U-notch roots were assumed to be semi-elliptical in shape with an a:c ratio of 1. The crack growth rate da/dN was then taken to be half the surface crack growth rate d(2c)/dN. ΔK at maximum depth for the short cracks was calculated using the equations outlined by Scott and Thorpe [31]. Instead of using the nominal far-field bending stress range to calculate ΔK, the local bending stress range in the notch root predicted by an elastic-plastic FE model was used. The resulting comparison on the basis of ΔK is displayed in Fig. 21. It is clear from Fig. 21 that ΔK alone is not a suitable parameter for characterising the U-notch short crack growth rates since it does not successfully collapse the data onto a single curve. The U-notch short cracks also exhibit some of the apparently "anomalous" behaviour of short cracks, namely growth at ΔK values below the long crack threshold and crack arrest events. There is also the fact that the short crack data exhibit relatively constant growth rates with increasing ΔK. However, the growth rate of Crack B tends towards the long crack data at higher ΔK, suggesting typical Stage II type crack growth behaviour at longer crack lengths.

3.5. Specimen lifetimes

Fatigue lifetimes to specimen fracture are listed in Table 2. The as-broached specimens exhibited the shortest lifetimes, with the σ_{max} = 790 MPa test resulting in a shorter life than the equivalent tests at 750 MPa. Testing in vacuum increased the fatigue lifetime by a factor of two at σ_{max} = 750 MPa. Polishing the surface of the U-notch resulted in an increase of the lifetimes in air at

σ_{max} = 750 MPa and 790 MPa. Again, testing at σ_{max} = 790 MPa resulted in a shorter lifetime than at σ_{max} = 750 MPa. For the interrupted tests in which replicas were taken from polished specimens, there was also an increase in fatigue life relative to the as-broached specimens, but the σ_{max} = 750 MPa and σ_{max} = 790 MPa tests had similar lifetimes.

4. DISCUSSION

4.1 Crack initiation by carbide oxidation

Experimental observations of eruptions and bulges associated with oxidised primary carbides strongly suggest that there is a substantial volume expansion when the primary carbides in IN718 oxidise. The volume expansion due to the transformation of NbC to Nb_2O_5 can be estimated using crystallographic data, although arriving at an estimate for the temperature range of interest (500-600°C) is complex, because Nb_2O_5 is polymorphic, existing in several different crystal structures at different temperatures. Amorphous Nb_2O_5 also exists and its density varies widely depending on the method of preparation. It is not known what form is adopted by the oxide eruptions in IN718, though a crystalline oxide form is considered to be more likely. For simplicity, just the oxidation of pure NbC to Nb_2O_5 will be considered. Using molar volume and density data for NbC [32] and Nb_2O_5 [33], estimates of the volume expansion factor will be calculated for the reaction:

$$4NbC + 9O_2 \rightarrow 2Nb_2O_5 + 4CO_2$$

Eqn. 1

The volume expansion factor is given by the expression:

$$\delta_V = \frac{V_{Nb_2O_5}}{2V_{NbC}}$$

Eqn. 2

where V_i is the molar volume of phase 'i'. Estimated volume expansion factors are listed in Table 3. The lower bound is 1.96, based on data for the B-form of Nb_2O_5, while the upper bound is 2.38, based on data for amorphous Nb_2O_5.

Using calculations based on work by Starink et al. [34] and Lee et al. [35], the misfit stresses due to the difference in volume between NbC and Nb_2O_5 can be calculated for primary NbC carbides oxidising to Nb_2O_5 in a matrix of IN718. This continuum mechanics model is outlined in Appendix A. The resulting estimates for the plastic zone radius around an oxidised NbC particle are listed in Table 4. This idealised case produced estimates of the plastic zone size r_p of between 3.91 and 4.30 times the untransformed particle radius r_{NbC}. Measurements were made on images of cross sections of oxidised particles and the corresponding bulges to compare the extent of deformation to the radii of the associated oxidised primary carbide particles. We estimated that the boundary between elastic and plastically deformed matrix is situated at points at which the bulge is about 10% of its maximum height. From these experimental observations, estimates of plastic zone ranging from 1.6 to 3.4 times the particle radius were obtained, with a mean value of 2.3. This is not a rigorous comparison, bearing in mind that (i) the plane of observation was generally not through the exact centre of the particle, (ii) the particles were close to the surface and hence the matrix was not infinite, (iii) in fatigue specimens, the strain due to loading may

have affected bulge formation and (iv) the particles in real specimens were not spherical. Especially the first two points will cause the measured estimates of r_p/ r_{NbC} to be lower than the calculated ones, by an amount that depends on the position of the particle relative to the plane of cross section and the sample surface. In view of this, the experimental observations are considered to be consistent with the calculations, thus supporting, semi-quantitatively, the theoretical predictions of the stresses and plastic deformation created when primary carbides oxidise and expand.

Given the experimental observations and the theoretical prediction of localised plastic deformation around oxidising carbides, the following mechanism of crack initiation in the U-notch fatigue specimens is proposed. The misfit strains due to primary carbide oxidation are superimposed on the elastic-plastic strain field in the U-notch due to external loading. This creates local strains high enough to cause rupture of the matrix in the vicinity of an oxidising particle, hence initiating a fatigue crack. The stress concentration effect of the notch root may promote stress-assisted oxygen diffusion, causing more rapid oxidation of the sub-surface primary carbides than that observed for unstressed thermal exposure specimens. Once a crack initiates, the crack itself may provide another fast oxygen diffusion route to a sub-surface particle. The high incidence of bulges at crack initiation sites suggests that expansion of oxidising sub-surface primary carbides is a significant mechanism of fatigue crack initiation in the notch root. It was the oxidised sub-surface carbides, rather than oxide eruptions in general, that were the more numerous crack initiation site in U-notch specimens tested in air. The incubation period at the start of the fatigue tests in which no cracks were observed probably arose because time was required for the carbides to oxidise. Additionally, IN718 is a material which exhibits planar slip at elevated temperatures, so the incubation period is consistent with the development of pre-initiation fatigue damage accumulation such as slip bands. The decrease in initiation rate later in the fatigue tests was possibly caused by exhaustion of the available nucleation sites. The number of cracks observed was also affected by coalescence events, so that the increase in crack number due to fresh nucleation was offset by the reduction in the number of cracks due to coalescence.

Crack Propagation

Disregarding temporary arrests, short cracks in the notch roots exhibited fairly constant crack growth rates. This is in contrast to the usual trend of increasing growth rate with increasing crack length observed for long crack tests [5 - 14]. The constant growth rate of isolated short cracks in the notch root suggests that the driving force for crack growth was constant. This cannot be successfully characterised using single unadjusted LEFM parameters like ΔK or K_{max} which indicate an increasing driving force with increasing crack length. In such situations it is common to consider crack closure to explain anomalous crack growth behaviour [36]. Crack closure arises when there is contact between crack faces in the wake of a growing crack, resulting in some load transfer. Load transfer reduces the effective crack driving force at the tip, with a consequent reduction in fatigue crack growth rates. Closure can be due to the combination of shear components causing plastic deformation at the crack tip and roughness (so called plasticity-induced or roughness-induced closure), or due to build-up of an oxide layer on the crack faces. In the case of the short cracks in U-notch specimens in this study, significant oxide-induced crack closure is considered to be unlikely. It was observed that crack propagation in air was partly intergranular, whereas in vacuum it was transgranular. This is consistent with the established theory of oxidation embrittlement of grain boundaries leading to enhanced crack propagation rates in IN718 at elevated temperatures. Hence in the U-notch specimens accelerated short crack

propagation due to oxidation embrittlement is thought to outweigh any closure effects due to the build-up of oxide on crack surfaces. The plastic zone in the notch root may have affected crack propagation, but plasticity-induced closure, like oxide-induced closure, is considered unlikely for the short cracks in the notch root. Some temporary crack arrest events were observed and there were a number of non-propagating or slowly propagating cracks. These arrests were more likely due to shielding and interaction with other cracks as described in the results section above. Plasticity-induced closure as an explanation of non-propagating cracks seems unlikely, bearing in mind many were typically less than 2c = 100 μm in length with limited crack wakes.

Sadananda and Vasudevan considered the anomalous behaviour of short cracks and as an alternative to closure theories proposed a two-parameter model for characterising crack growth rates [37, 38, 39, 40]. Briefly, their approach states that for a given crack growth rate, there are two driving forces, ΔK and K_{max}, which must be sufficient for cracks to grow. ΔK accounts for the accumulation of cyclic plasticity in the material and K_{max} (or its EPFM equivalent J_{max}), accounts for the forces required to break crack-tip bonds and cause crack advance. This leads to two crack growth thresholds, ΔK^* and K^*_{max} which must both be exceeded if a crack is to propagate. Short crack growth behaviour such as arrest was explained by arguing that the local value of K_{max} is affected by "internal stresses" [38], such as the stress field of a notch, dislocation density gradients, or stress concentration at a slip band extrusion. Sadananda and Vasudevan proposed [37, 38, 39, 40] that for short cracks it is the local crack tip environment that is crucial for determining crack propagation, and hence K_{max}, rather than ΔK is the important driving force for crack growth. For long cracks, the sensitivity to local crack tip conditions decreases and crack growth behaviour is controlled by ΔK. Sadananda and Vasudevan demonstrated [37] it was possible to rationalise the anomalous behaviour of short cracks without invoking closure theories, though this is considered to be a controversial position (see footnote to reference [37]). Their approach is interesting because it acknowledges the importance of the local crack tip environment for determining crack growth behaviour. A different two-threshold approach was discussed by Miller, who also acknowledged the importance of local conditions, in particular microstructure, in determining crack growth. [41]. He characterised fatigue behaviour in terms of a microstructural threshold which was important for short cracks, and a mechanical threshold which applied for long cracks. For the short cracks observed in this study, a clear source of the internal stresses postulated by Sadananda and Vasudevan is the mis-match caused by the oxidation of primary carbides. This will drive crack initiation and the early stages of crack propagation, and may explain why some cracks arrested as they grew away from the region of high local stresses at the initiation site. However, other cracks did not arrest and continued to grow at a fairly constant rate, suggesting other influences on crack driving force. Tests were conducted at 0.25 Hz (1-1-1-1 waveform) at 600^{o}C in air, so the time-dependent processes of oxidation and creep will operate in IN718. On a microstructural scale, oxidation will tend to accelerate crack growth through grain boundary embrittlement, thereby reducing the local threshold for crack growth. In a competing process, stress relaxation at the crack tips during dwell may reduce the local driving force available to propagate the cracks. As cracks grow, the local environment of each crack tip will vary depending upon a number of factors, such as the position of the crack in the notch stress-strain field, shielding by other cracks, microstructural features such as grain boundaries, broaching marks (in the case of as-broached specimens) and the possible influence of the work-hardened deformation layer caused by broaching. However, there remains the difficulty of calculating the local driving force for individual cracks when the contributions of these different factors are unknown or difficult to model.

It is thought that the hardened deformation layer present in U-notch specimens prior to fatigue testing influenced crack initiation and propagation. All the cracks observed had the characteristic of being straight and transgranular at the surface. Below the notch surface, there was a transition from a flat fracture surface to rougher mixed transgranular-intergranular cracking, shown in Fig. 20. The depth at which this occurred was 30-50 μm, greater than the visible depth of the surface deformation layer, but perhaps at the boundary of the region of material affected by the broaching process.

Later in the fatigue life, once cracks had reached several hundred microns in length, there was a transition to very rapid crack growth, assisted by crack coalescence. This rapid crack growth at the end of the fatigue tests accounted for 6% of the life at σ_{max} = 750 MPa and 17% of the life at σ_{max} = 790 MPa. Another study of fatigue crack propagation in a similar notch geometry was performed by Bache et al. [15]. They used double edge U-notch bend specimens with a quoted stress concentration factor of 2.23, to study low cycle fatigue crack propagation at 600°C. Rather than naturally initiated cracks, single pre-initiated cracks (typically 2c = 1mm) were studied. Very rapid, accelerating crack growth rates were reported, with cracks approaching critical dimensions (2c ≈ 8mm) within 2000 cycles [15]. It appears that by considering different crack length scales, the observations of Bache et al. [15] and the results presented here are complementary. For naturally initiated short cracks, there is a period of stable crack growth, until a critical crack size is reached and there is a transition to rapid crack growth in which the growth rate increases with increasing crack length.

Fatigue Lifetimes

Polishing the U-notch to remove broaching marks resulted in a pronounced increase in fatigue life for a 1-1-1-1 cycle at 600°C in air. A similar trend was previously reported for U-notch specimens of extruded IN718, tested using a 10 Hz sawtooth waveform in air at 600°C [25]. Removal of the broaching marks may reduce crack initiation due to micro-notch effects, though cracks still initiated early in the fatigue life due to carbide oxidation. An alternative possibility is that the broaching marks enhanced surface crack propagation, since they are favourably oriented parallel to the crack growth direction.

The interrupted polished notch tests at σ_{max} = 750 MPa and 790 MPa produced similar lifetimes of 51279 and 51687 cycles respectively. One would have expected the higher stress level to have produced a shorter fatigue life, as was the case for the uninterrupted tests. However, fatigue lives typically exhibit some scatter and the observed lifetimes may reflect this inherent variability. The majority of the specimen life was taken up by the growth and interaction of numerous short fatigue cracks, until coalescence of several cracks generated a dominant defect which propagated rapidly to failure. The dominant cause of crack initiation was primary carbide oxidation, so crack distribution will be affected by the number density and spatial distribution of primary carbides at the notch root. The rate of crack nucleation will depend upon the rate of primary carbide oxidation, which in turn is affected by the depth of individual carbides below the surface, their proximity to preferential oxidation diffusion pathways such as grain boundaries, and hence the rate of oxygen diffusion to them. The plastic strain in the notch root due to external loading is not uniform, so that the local matrix strain around an oxidising particle will vary according to its position relative to the notch axis. Spatial variation in strain amplitude with position will also influence crack propagation, as will the proximity of other short cracks which could result in

shielding or coalescence. This is illustrated by the rapid propagation of Crack II in the σ_{max} = 750 MPa test. It was located close to the notch axis, and initially grew in isolation away from the influence of other cracks.

The lifetime of the specimens may also have been affected by the transition from stable short crack growth to rapid growth and crack coalescence. For σ_{max} = 750 MPa, stable growth continued until 48000 cycles, when Crack II was 842 μm in length. Beyond this point, coalescence and growth was very rapid and by 50000 cycles there was a crack 8.7 mm long running to one end of the U-notch. For σ_{max} = 790 MPa, the transition from stable crack growth to rapid growth and coalescence occurred at 43000 cycles, when the longest crack (Crack A) was 301 μm in length. This shorter length at the transition point may have been a consequence of the higher load level.

CONCLUSIONS

Oxidation of (Nb,Ti)C primary carbides in IN718 readily occurs at temperatures of 550-600^{o}C in air, and a substantial volume expansion occurs as a result of oxidation. Calculations of the misfit between an oxidised primary carbide and the surrounding matrix predict that the misfit strains are high enough to cause localized plastic deformation of the matrix. Direct evidence of such plastic deformation was observed in unstressed thermally exposed specimens and in U-notch fatigue specimens tested at 600^{o}C.

Bulge-like crack initiation sites associated with oxidised sub-surface primary carbides indicate that initiation is due to the mismatch strains between the oxidising particle and the surrounding matrix. The mismatch strains are superimposed on the stress-strain field due to external loading, resulting in deformation high enough to cause localized rupture of material in the notch root, hence initiating a fatigue crack.

The surface cracks in the U-notches were all remarkably straight, with no deflections except those occurring during crack coalescence. Unlike long cracks, the propagation of naturally initiated short surface cracks in the U-notch root was observed to be approximately constant across a wide range of crack lengths. Arrest or retardation of growing cracks could be attributed to shielding by other cracks in the vicinity. However, there was a transition to rapid, accelerating crack growth towards the end of the fatigue life, once cracks had reached several hundred microns in length. Rapid propagation in the latter stages of the fatigue life was assisted by crack coalescence.

Fatigue lifetimes were affected by notch surface condition. Polishing the notch to remove broaching marks had a beneficial effect on fatigue life.

ACKNOWLEDGEMENTS

This work was funded by the United Kingdom Engineering and Physical Sciences Research Council and ALSTOM Power. The authors wish to thank Dr. R. Jakeman, Dr. S. J. Mossp and M. Hughes of ALSTOM Power for valuable technical discussions and provision of the IN718 material.

TABLES

Element	wt%
B	0.0029
C	0.031
N	0.0059
O	0.0006
Mg	0.0017
Al	0.46
Si	0.08
P	0.01
S	0.0004
Ti	1.02
Cr	17.99
Mn	0.06
Fe	18.64
Co	0.43
Ni	52.89
Cu	0.10
Mo	3.02
Nb + Ta	5.22

Table 1: Composition of Inconel 718 disc forging.

Test Conditions	σ_{max}	
	750 MPa	790 MPa
Broached notch. Air. Uninterrupted.	23056*	8792
Broached notch. Vacuum. Uninterrupted.	53412	-
Polished notch. Air. Uninterrupted.	169413	50373*
Polished notch. Air. Replicas every 2000 cycles.	51279	51687

Table 2: Lifetimes of U-notch specimens. * denotes average of two tests.

Phase	Density (g cm^{-3})	Molar Volume (cm^3 mol^{-1})	Estimated volume expansion factor
NbC	8.18	12.83	n/a
H – Nb_2O_5	4.55	58.42	2.28
B – Nb_2O_5	5.29	50.2	1.96
Amorphous Nb_2O_5	4.36 - 5.12	51.9 - 61.0	2.02 - 2.38

Table 3: Estimated volume expansion factors for the oxidation of pure NbC to Nb_2O_5. Density and molar volume data were obtained from references [32] and [33].

Oxide Phase	r_p/r_{NbC}
H-Nb_2O_5	4.22
B-Nb_2O_5	3.91
Amorphous Nb_2O_5	3.97-4.30

Table 4: Estimated plastic zone radii around an NbC particle which has transformed to Nb_2O_5.

FIGURES

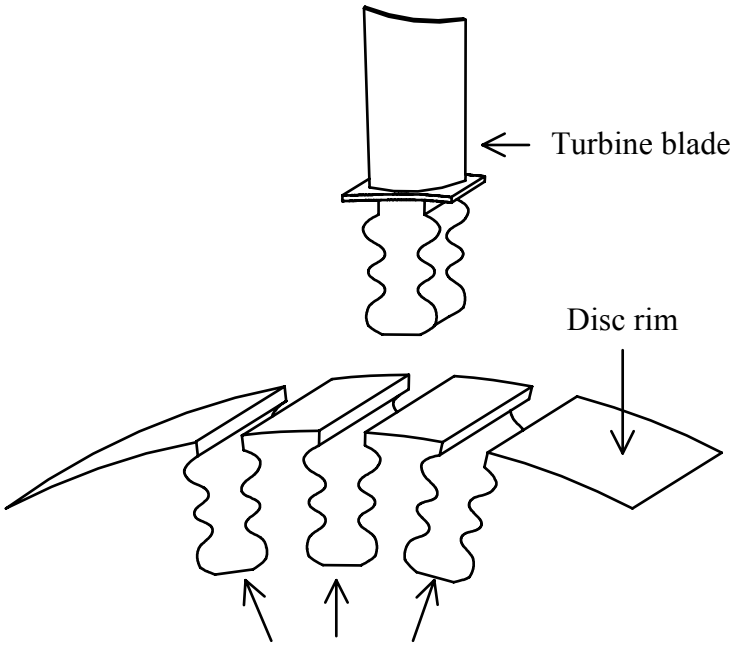

Fig. 1: Schematic diagram showing fir tree root fixings in a turbine disk rim.

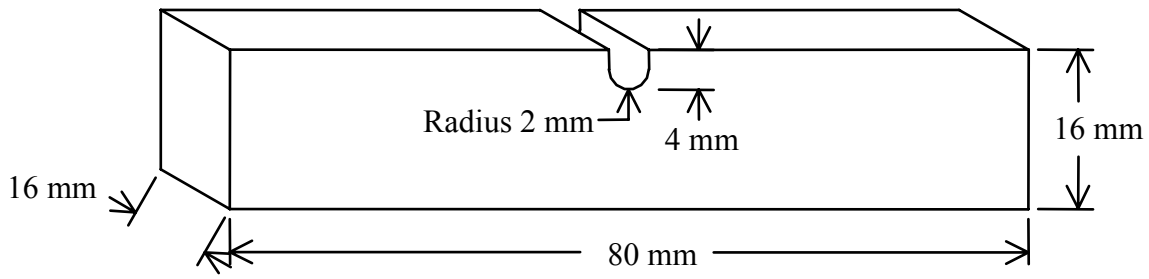

Fig. 2: U-notch specimen geometry.

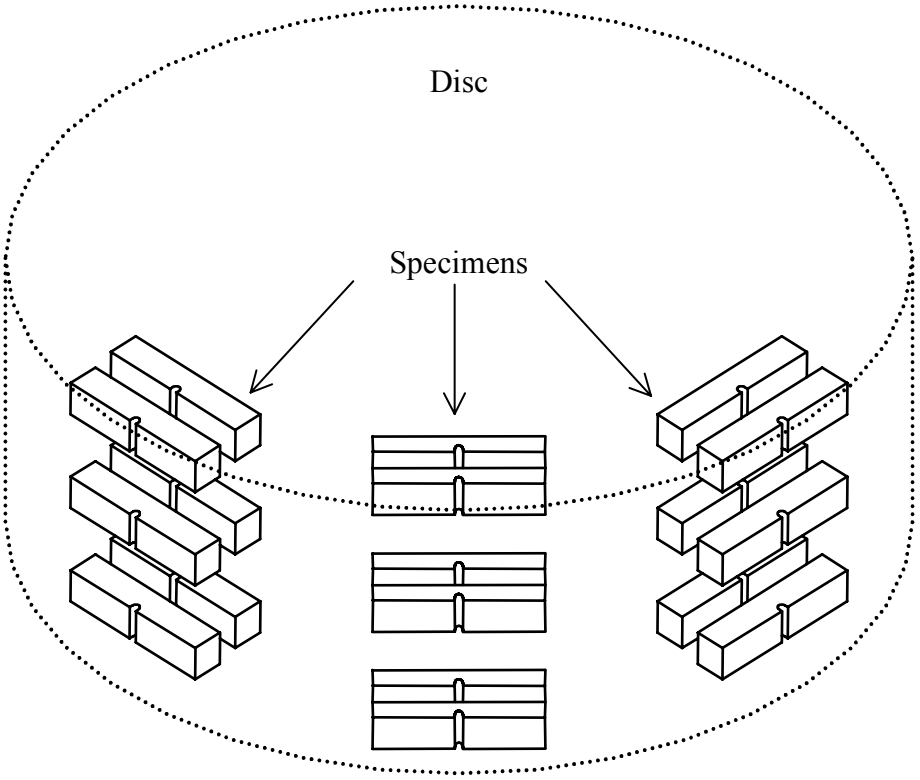

Fig. 3: Orientation of U-notch specimens extracted from IN718 disc forging.

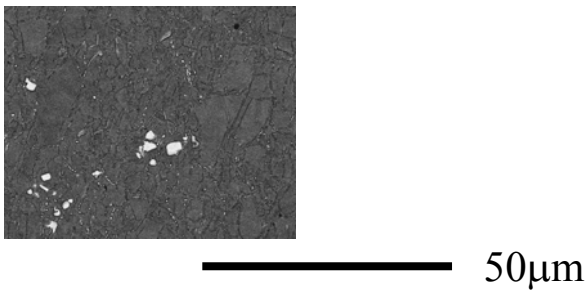

Fig. 4: SEM backscatter image of typical disc microstructure. The bright globular features are (Nb,Ti)C primary carbides. The small bright particles on the grain boundaries are δ phase.

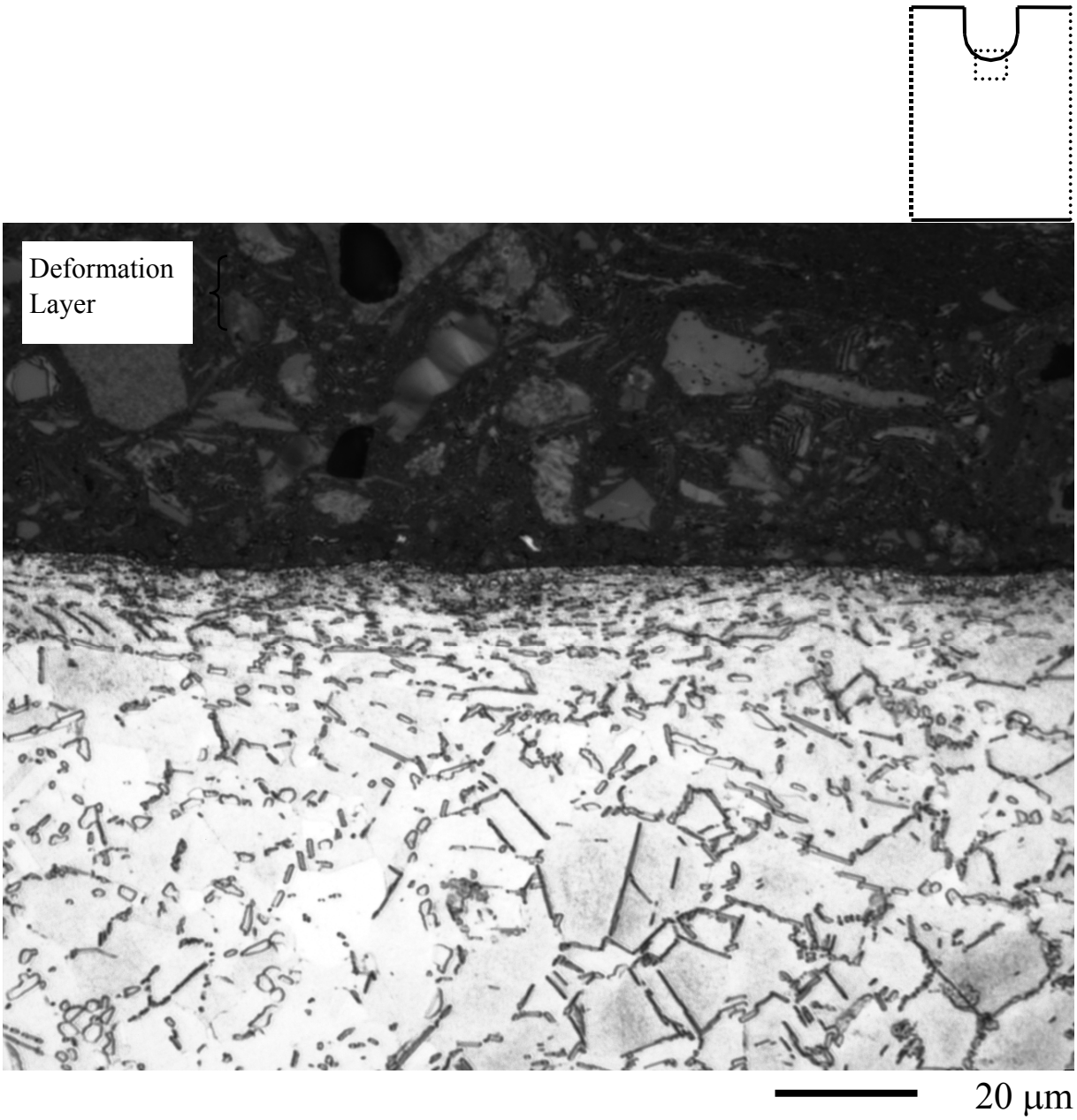

Fig. 5: Optical micrograph of section through a U-notch root, showing presence of a deformation layer at the surface.

Fig. 6: Tower-like eruptions of material from the oxidation of (Nb,Ti)C at the surface of a polished IN718 specimen exposed for 16 h at 550^{o}C.

Fig. 7: Irregular surface eruption of oxidised (Nb,Ti)C.

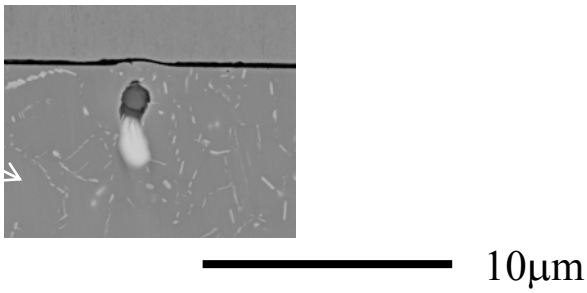

Fig. 8: Backscattered electron image, showing partially oxidised sub-surface primary carbide. Note the bulge in the surface above the particle.

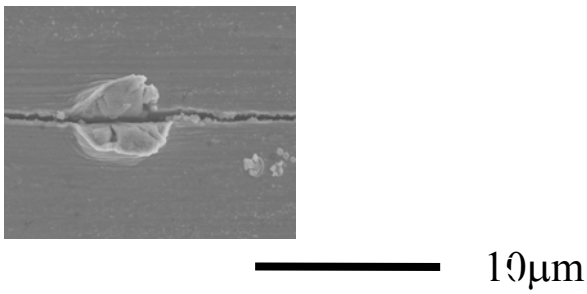

Fig. 9: Crack initiated at a surface eruption.

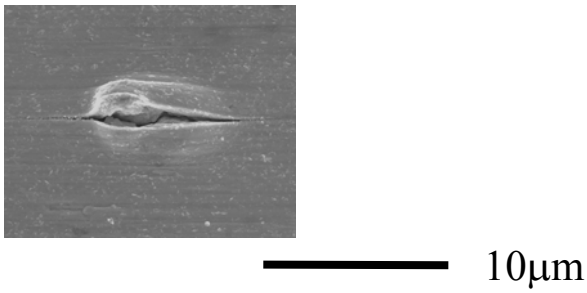

Fig. 10: Plan view of a short crack initiated at a surface bulge. The bulge was formed by the oxidation of a sub-surface (Nb,Ti)C primary carbide.

Fig. 11: Side view of a bulge in the notch root created by the oxidation of a sub-surface (Nb,Ti)C primary carbide. The horizontal marks are broaching marks.

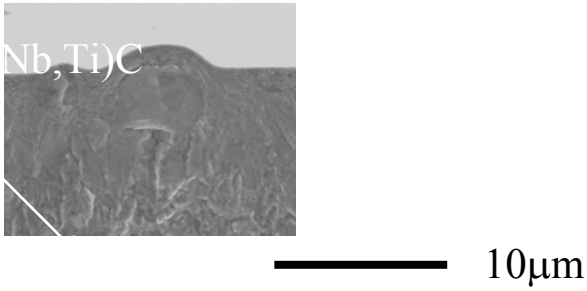

Fig. 12: Bulge-like crack initiation site on the main fracture face of a U-notch specimen. The particle below the bulge was identified by EDS as oxidised (Nb,Ti)C.

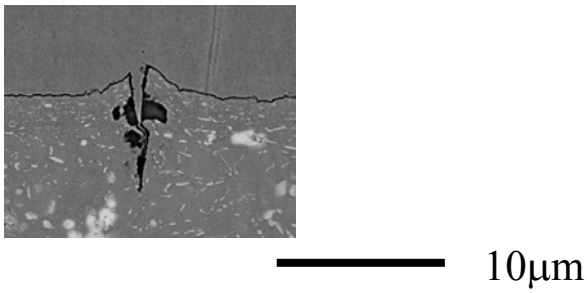

Fig. 13: Backscattered electron image of a metallographic section through a fractured U-notch specimen. The image shows a secondary crack in the notch root. Note the presence of the oxidised (Nb,Ti)C particle and the surface deformation above it.

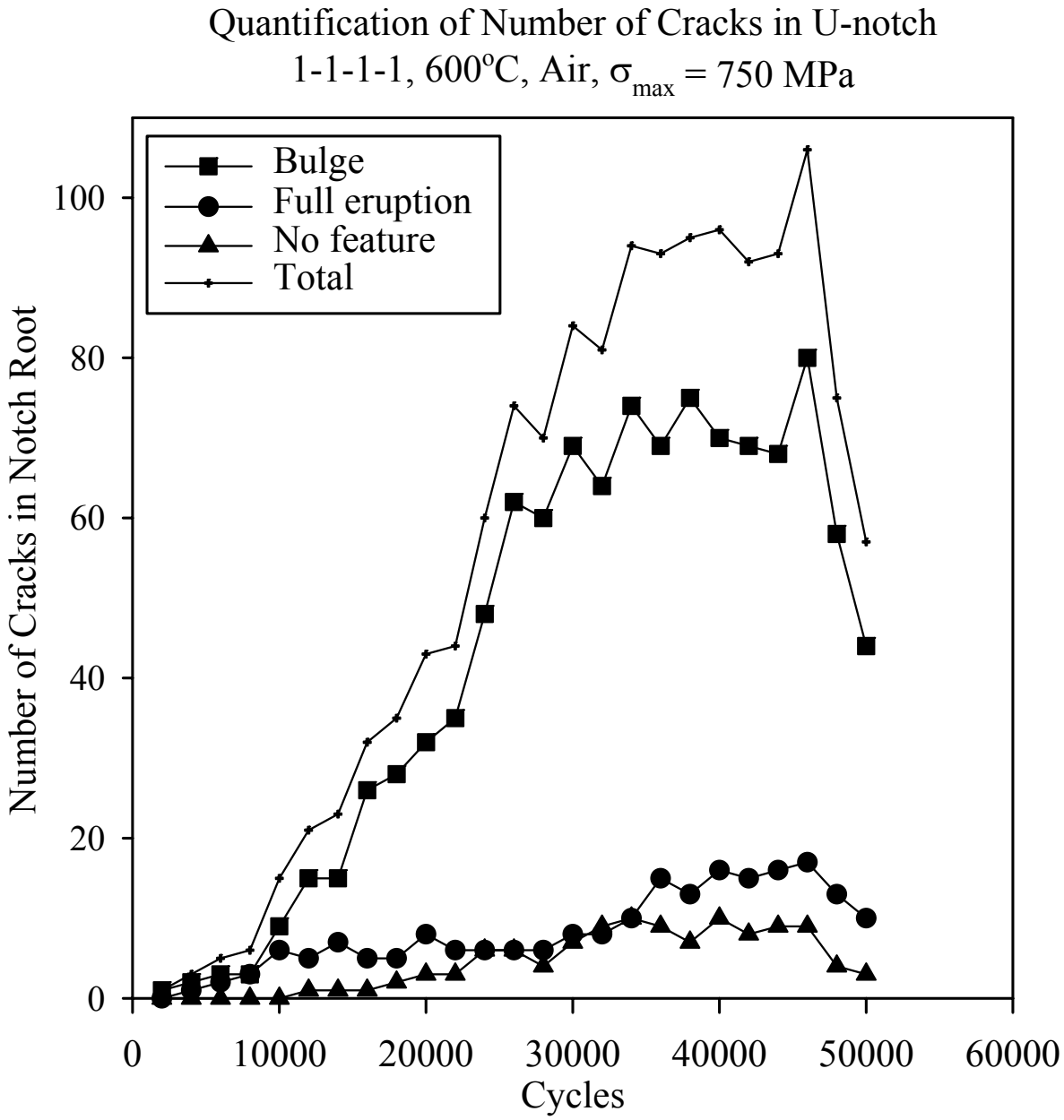

Fig. 14(a): σ_{max} = 750 MPa

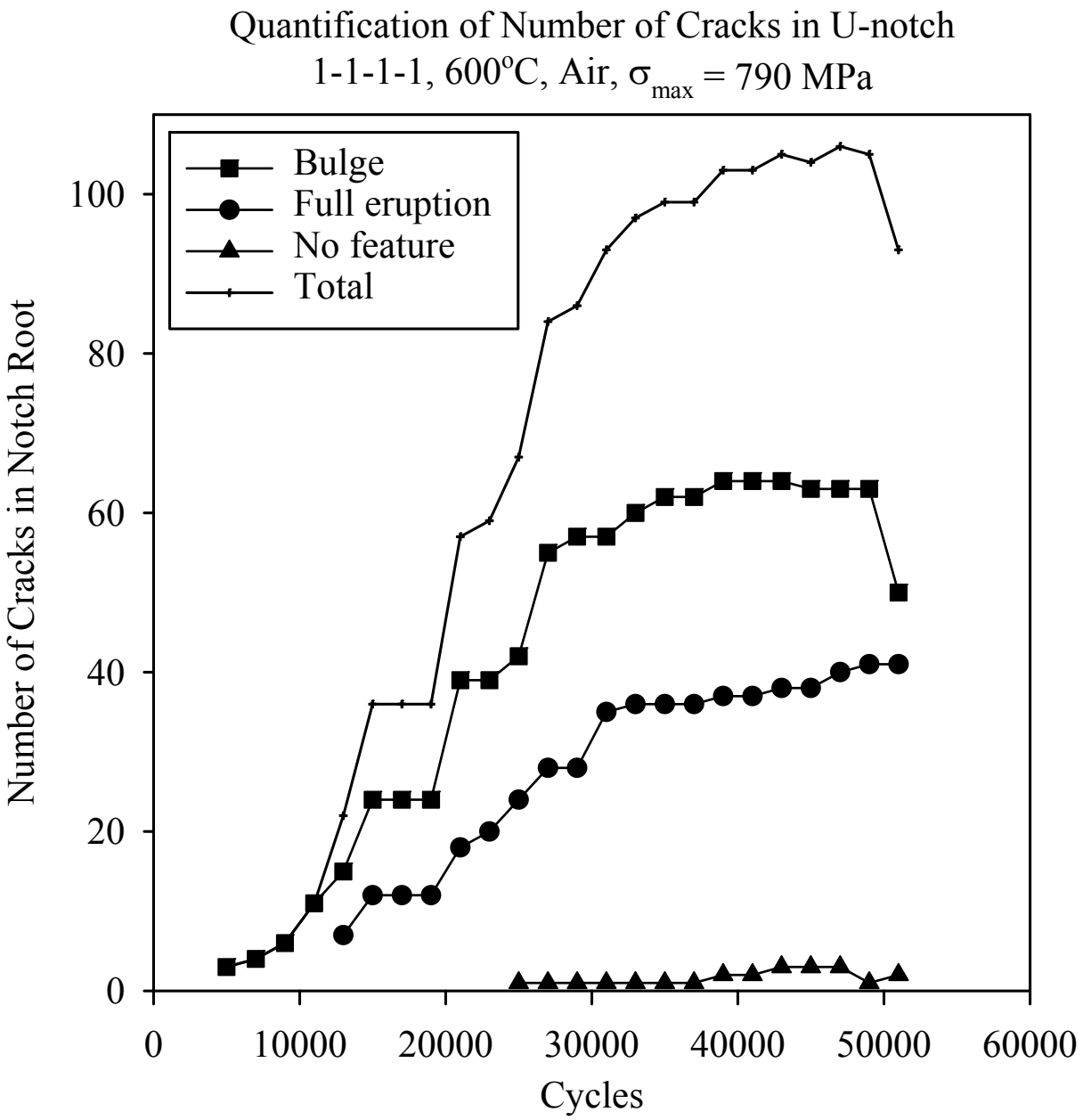

Fig. 14(b): σ_{max} = 790 MPa

Fig. 14: Quantification of number of cracks observed in notch root for two experiments performed on polished U-notch specimens: (a) σ_{max} = 750 MPa; (b) σ_{max} = 790 MPa.

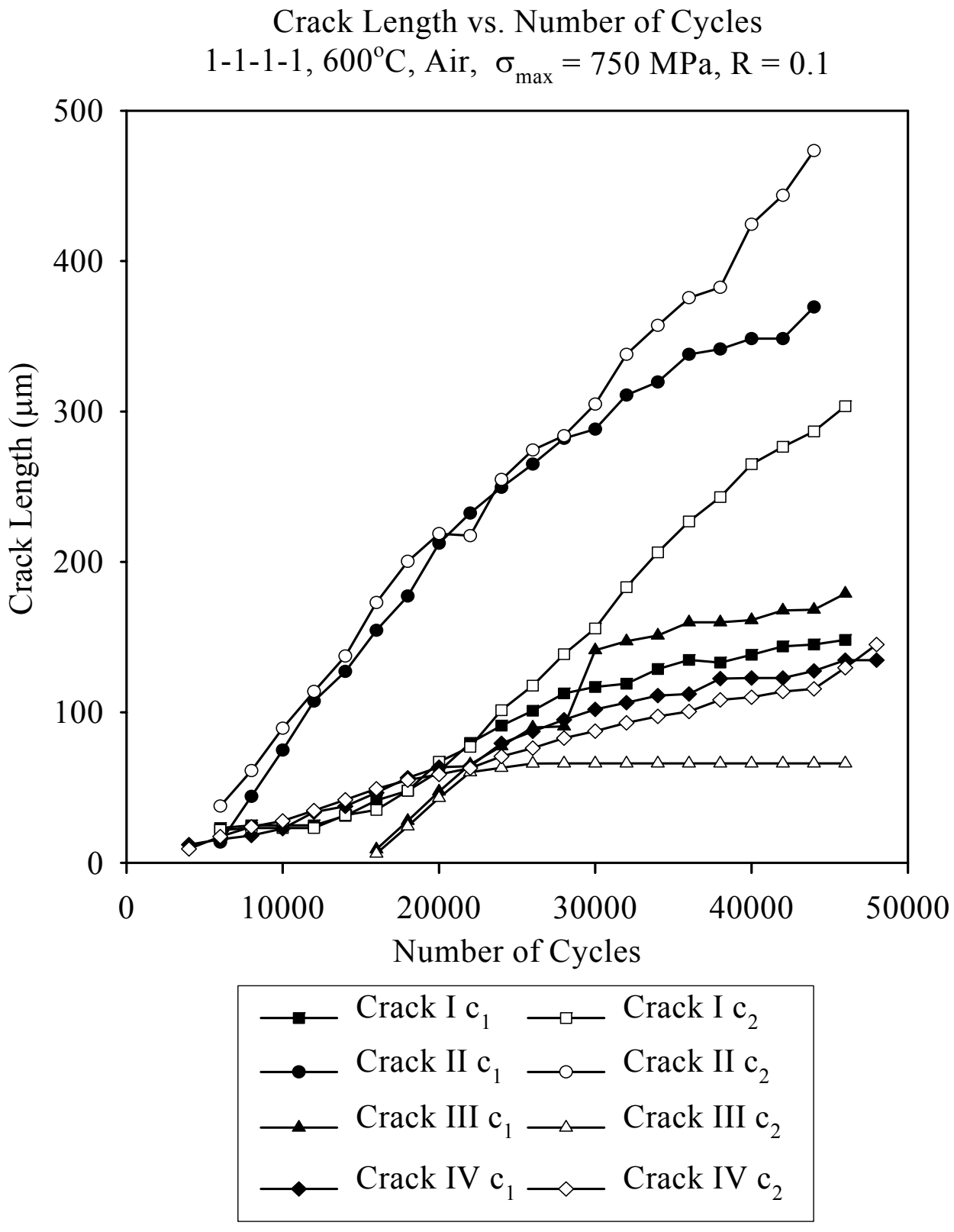

Fig. 15(a): σ_{max} = 750 MPa

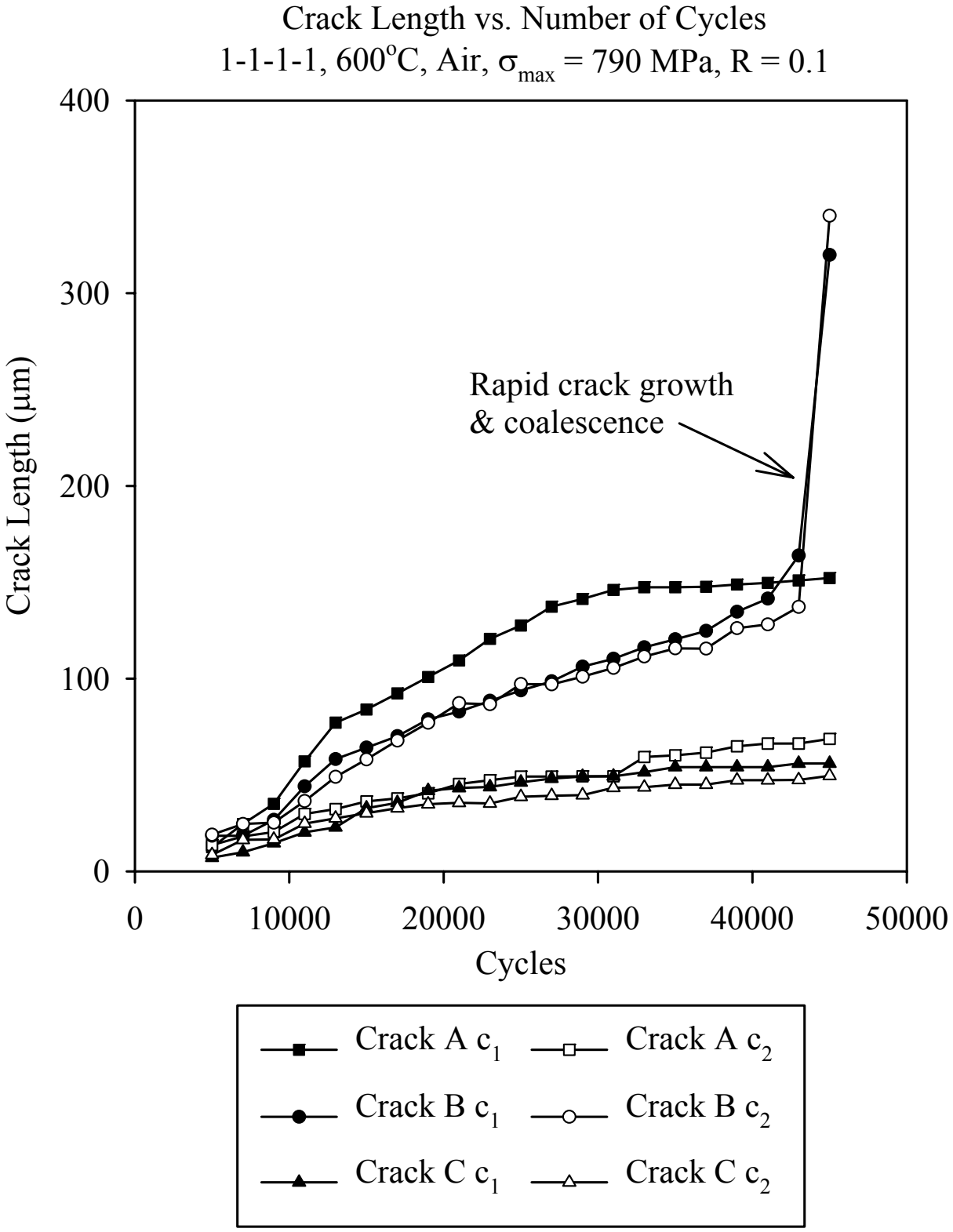

Fig. 15(b): σ_{max} = 790 MPa

Fig. 15: Short crack growth in the roots of polished U-notch specimens. (a) σ_{max} = 750 MPa; (b) σ_{max} = 790 MPa.

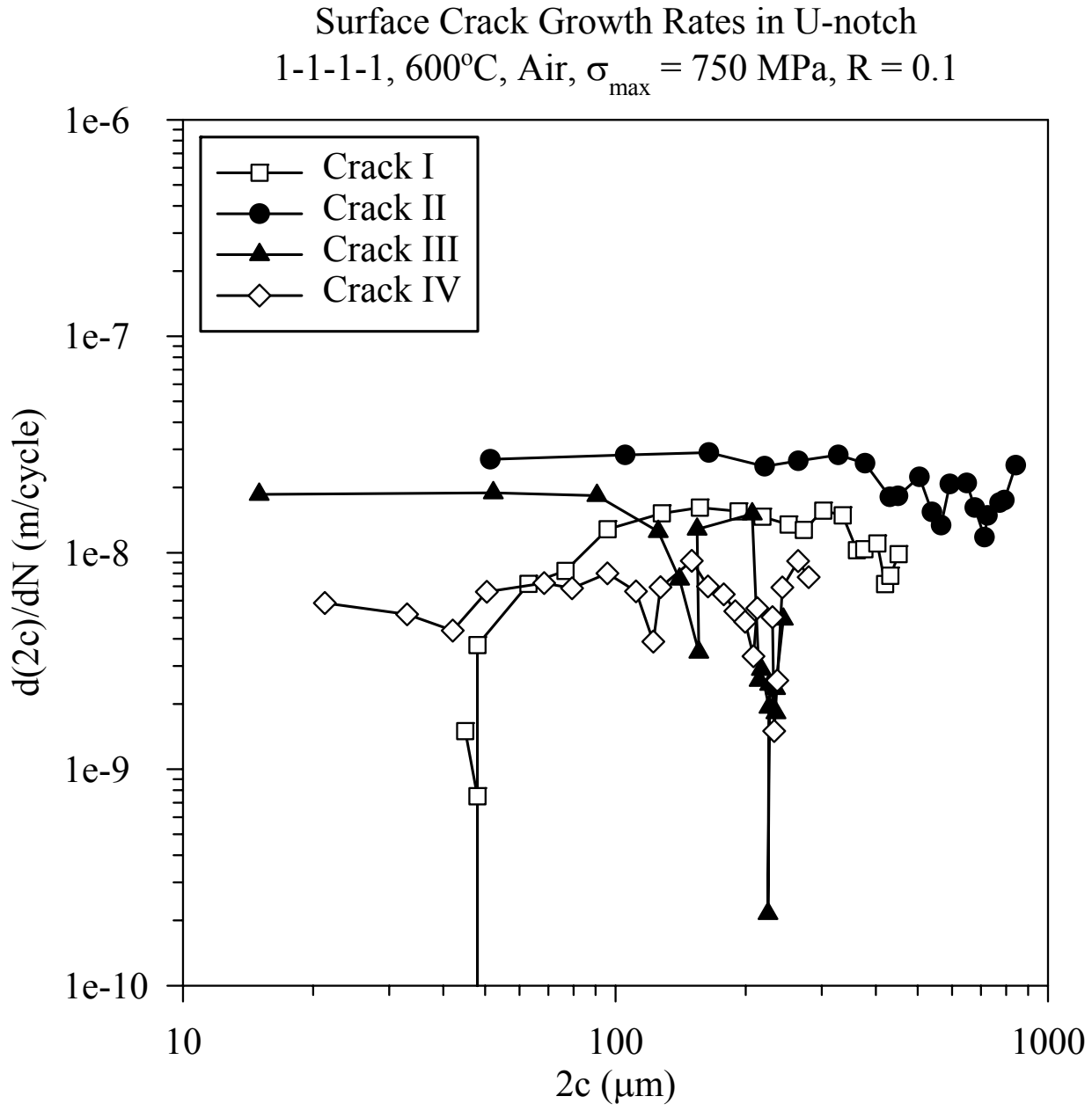

Fig. 16 (a): σ_{max} = 750 MPa

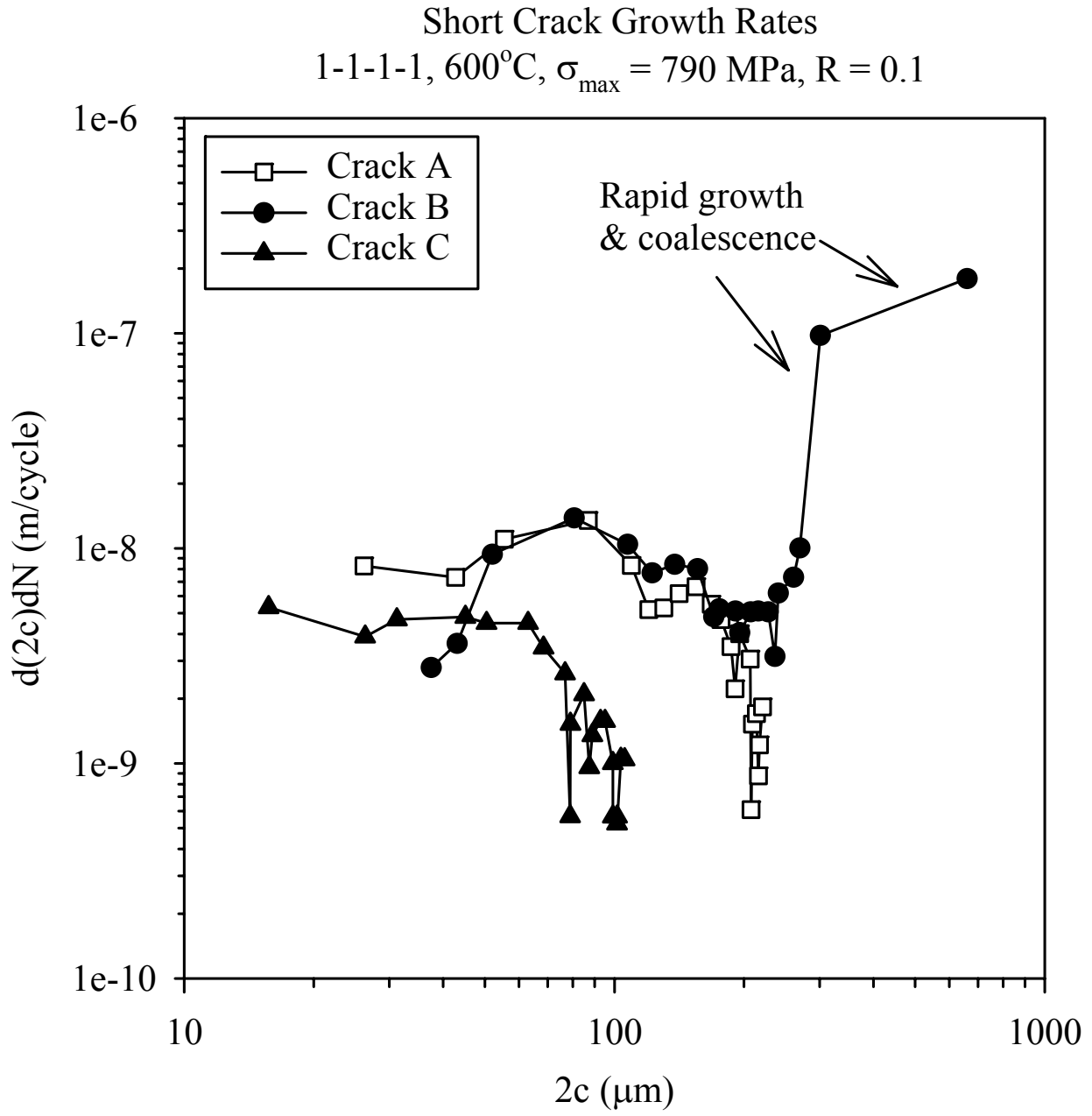

Fig. 16(b): σ_{max} = 790 MPa

Fig. 16: Short crack growth rates in the root of polished U-notch specimens. (a) σ_{max} = 750 MPa; (b) σ_{max} = 790 MPa

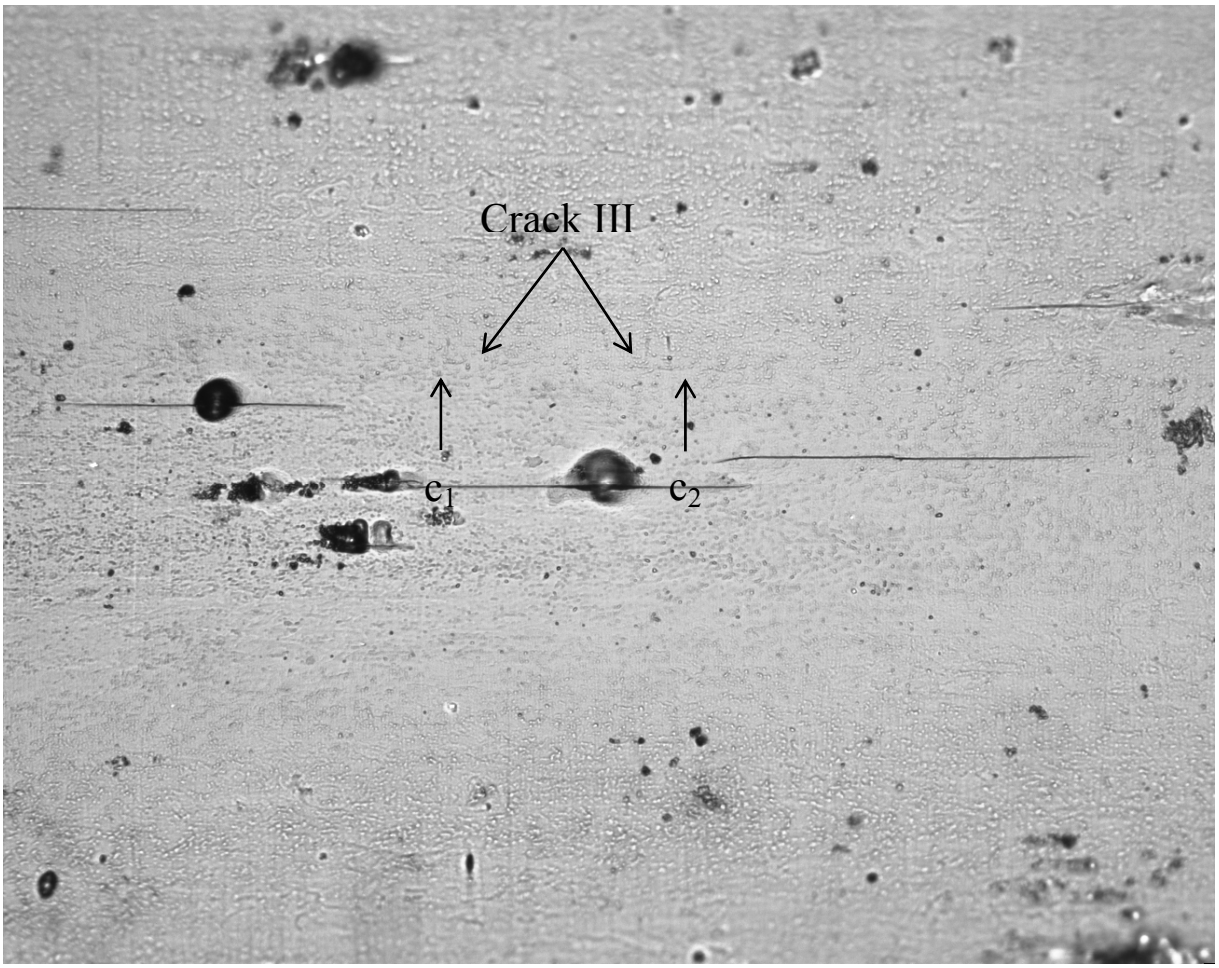

(a) 28000 cycles.

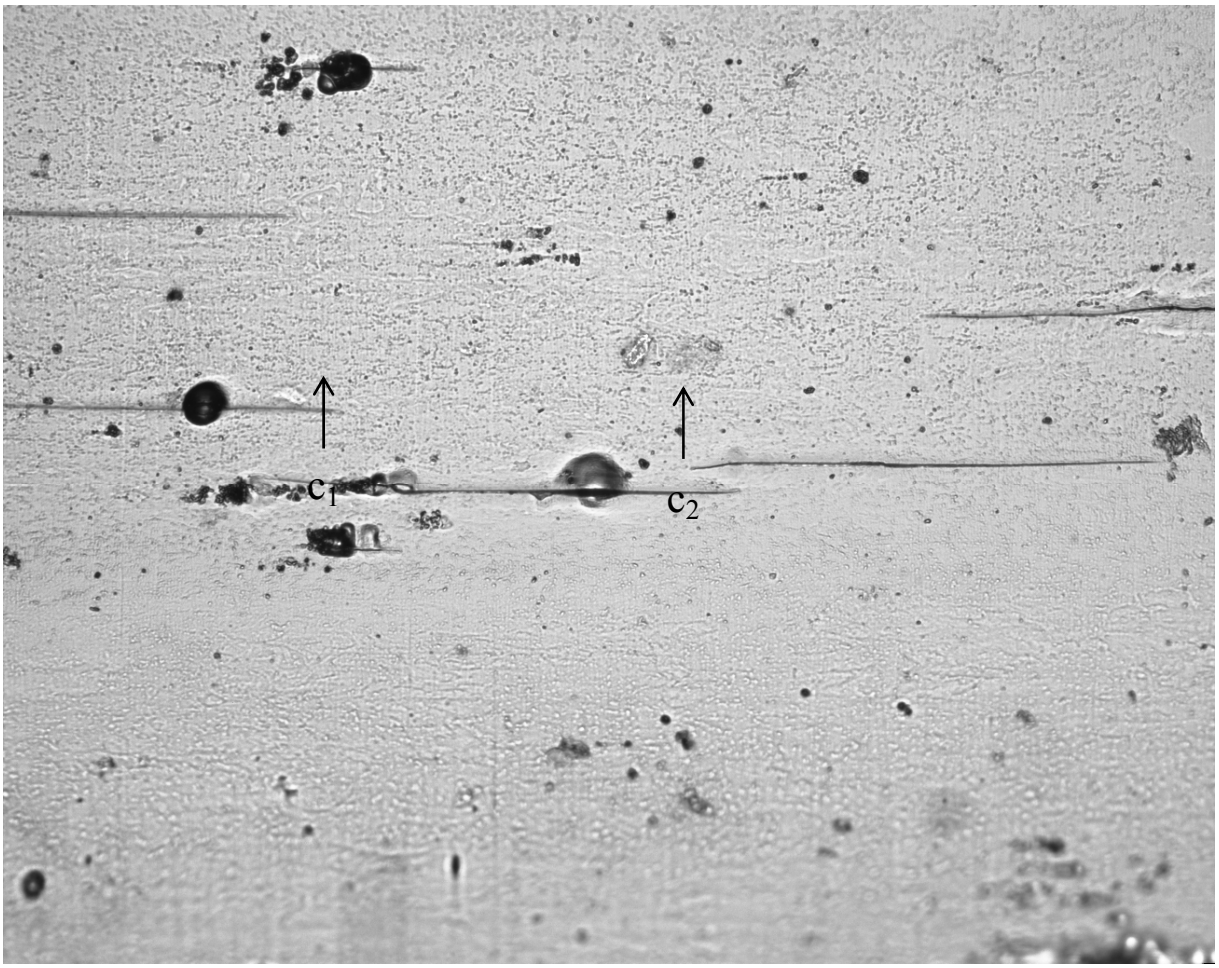

(b) 34000 cycles.

Fig. 17: Images from replicas showing arrest of one tip (c_2) of Crack III, while the other tip (c_1) continued to grow, assisted by coalescence. Note the bulge-like feature at the initiation site of Crack III. Test conducted with σ_{max} = 750 MPa, R = 0.1. The tensile axis is vertical.

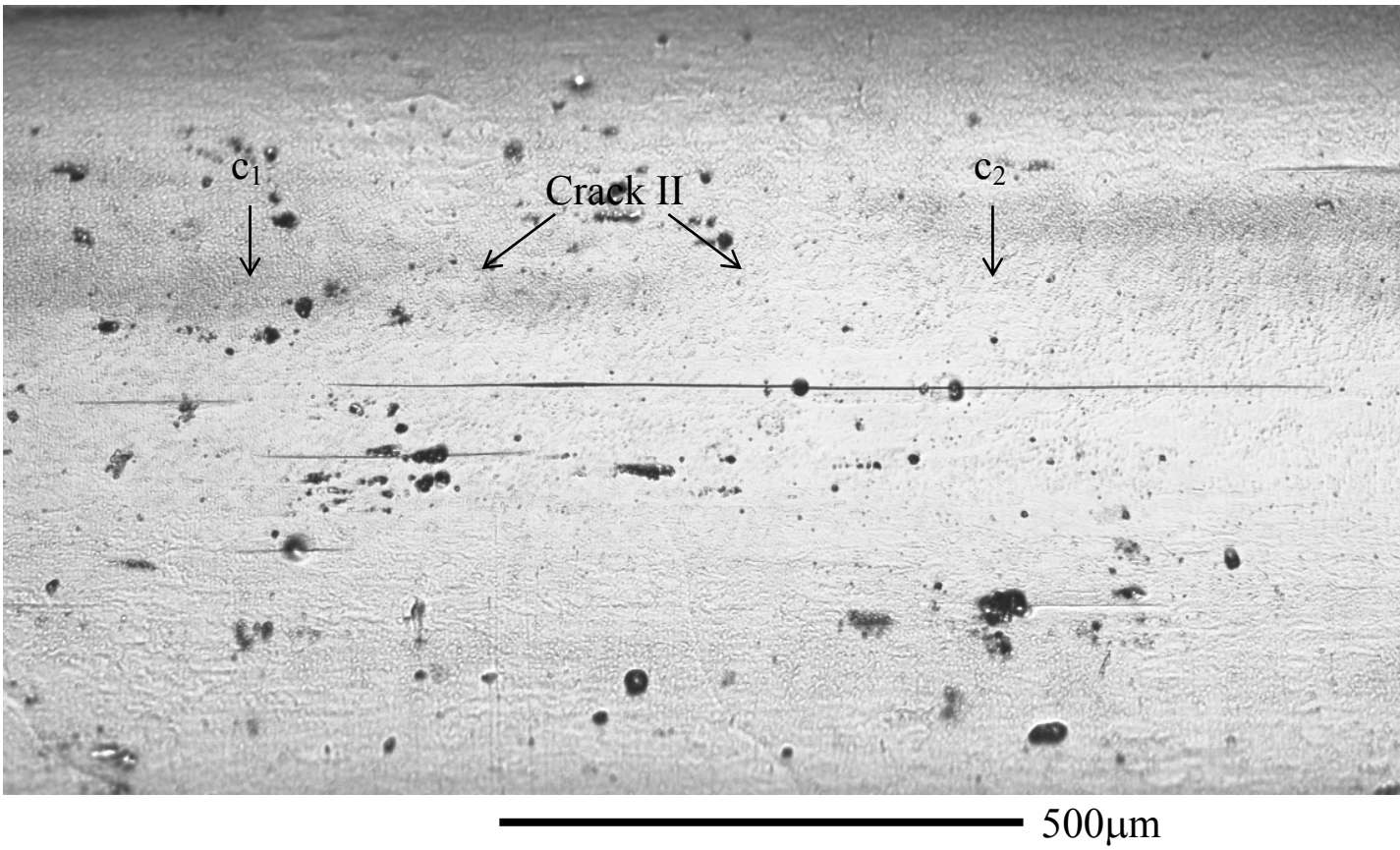

Fig. 18: Image of replica taken from U-notch root. The image shows Crack II from Fig. 15(a) and Fig. 16(a) after 36000 cycles. Segment c_1 of the crack was retarded due to shielding by other cracks. Test conducted with σ_{max} = 750 MPa, R=0.1. The tensile axis is vertical.

(a) 48000 cycles.

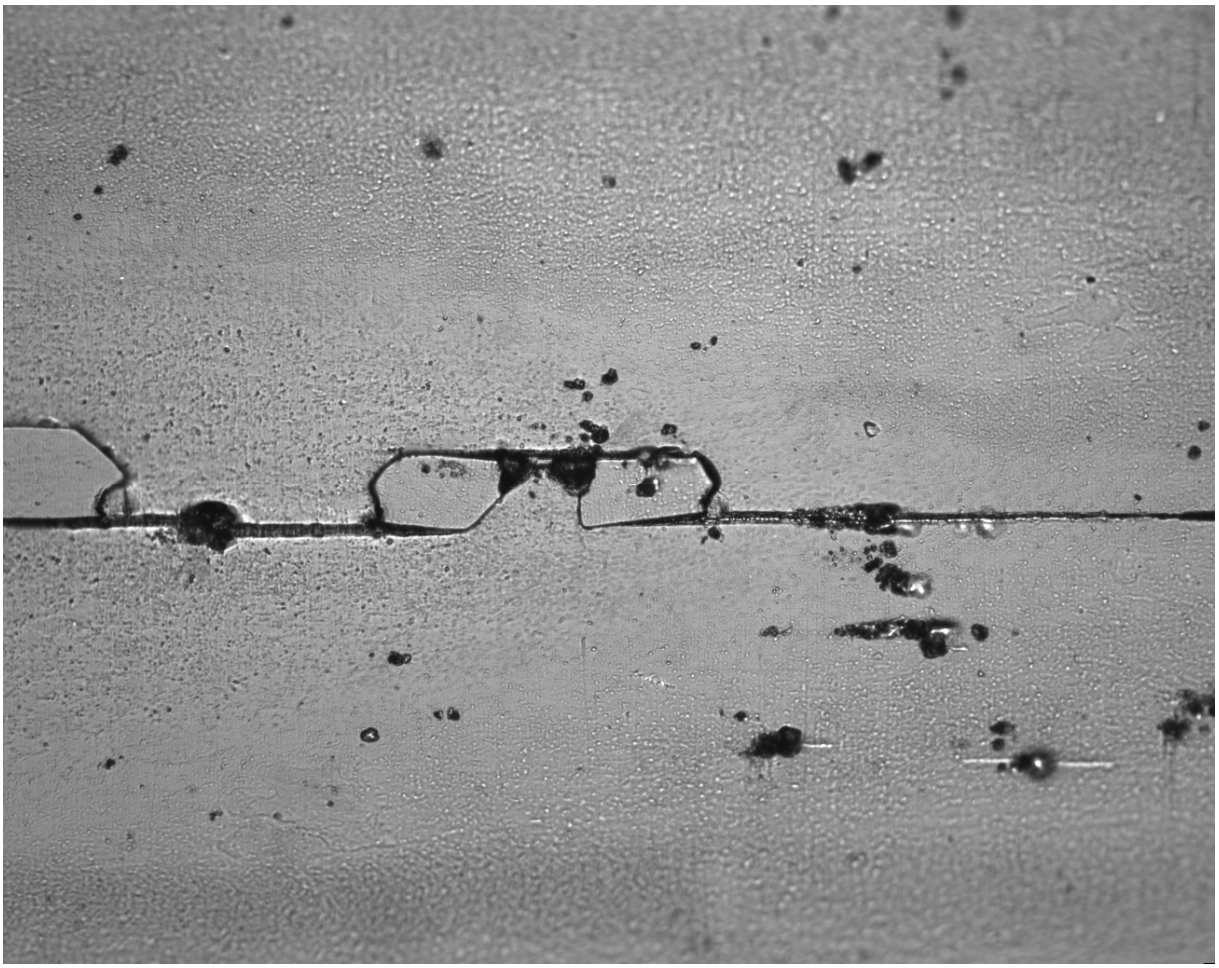

(b) 50000 cycles.

Fig. 19: Images from replicas showing rapid surface crack coalescence towards the end of the fatigue life. Test conducted with σ_{max} = 750 MPa, R=0.1.

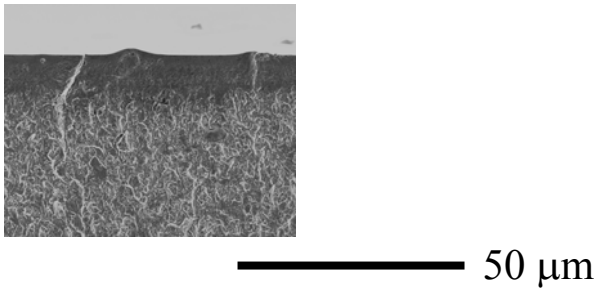

Fig. 20: SEM image of fracture surface, showing transition from transgranular to mixed-mode fracture in the specimen depth direction.

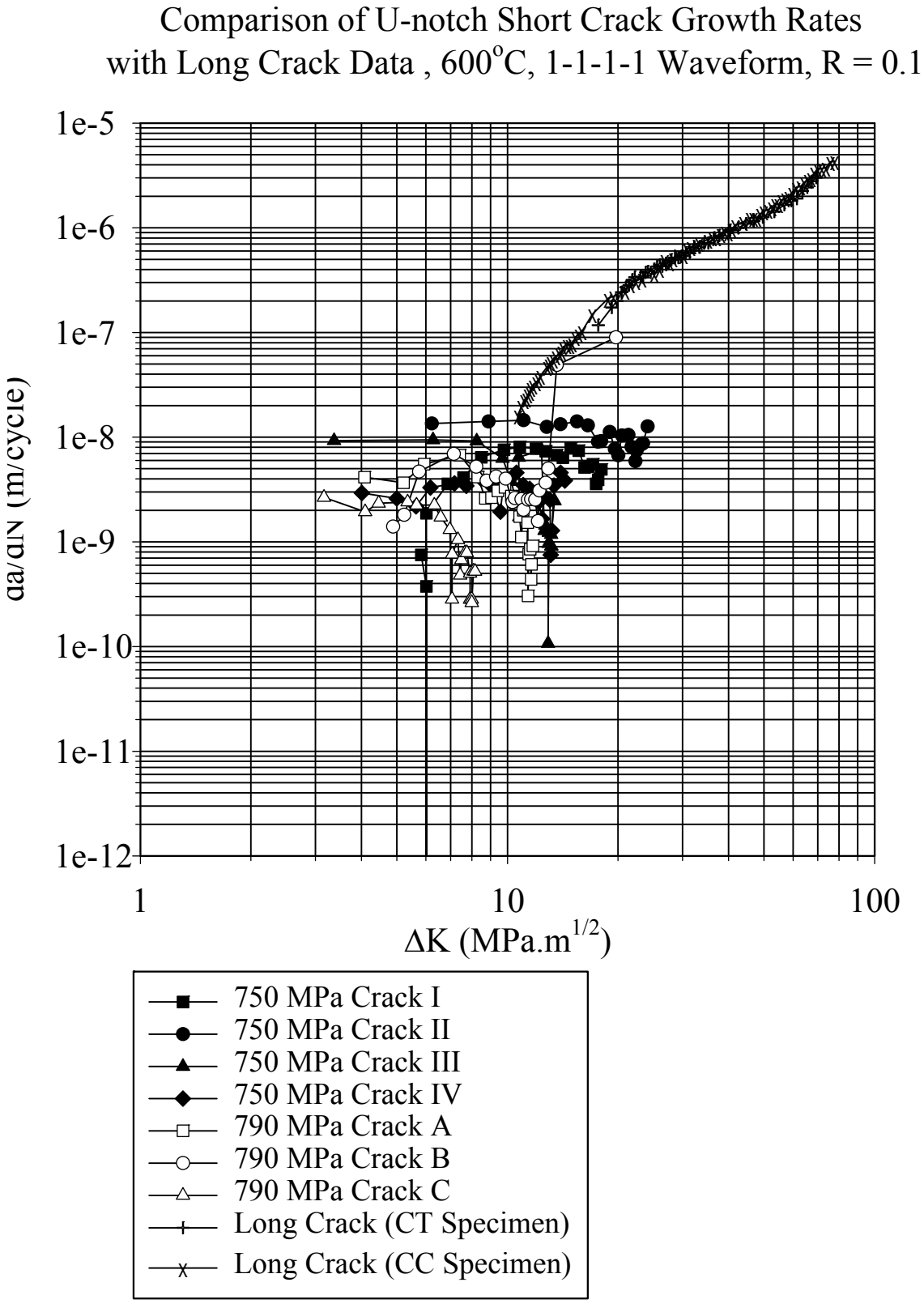

Fig. 21: Comparison of short crack growth rates in U-notches with long crack data obtained at 600°C using a 1-1-1-1 waveform and R = 0.1.

APPENDIX A

For a spherical inclusion 'B' in a continuous matrix 'A', the misfit parameter ε_m is defined as:

$$\varepsilon_m = \frac{r_{oB} - r_{oA}}{r_{oA}}$$

Eqn. 3

where r_{oB} and r_{oA} are the radii of the free undeformed particle 'B' and the empty undeformed cavity in the matrix 'A' respectively. For a spherical particle of NbC oxidising to Nb_2O_5, the misfit parameter is defined as:

$$\varepsilon_m = \frac{r_{Nb_2O_5} - r_{NbC}}{r_{NbC}}$$

Eqn. 4

Assuming a spherical particle of NbC of radius r_{NbC} oxidises completely to Nb_2O_5, then using the volume expansion factor calculated in Equation 2 gives:

$$\varepsilon_m = \sqrt[3]{\delta_V} - 1$$

Eqn. 5

Lee et al. [35] considered the case of a spherically misfitting inclusion in an infinite matrix, in which the matrix deforms plastically around the inclusion. Their model assumes that the matrix is a perfectly plastic material which obeys the von Mises yield criterion. The following expressions for the stress components (in polar co-ordinates) are obtained for a particle of radius r_B:

$$\sigma_r = \sigma_\theta = p_B \qquad r < r_B$$

Eqn. 6

$$\sigma_r = \sigma_\theta - \sigma_y = 2\sigma_y \ln\left(\frac{r}{r_B}\right) + p_B \qquad r_B \le r \le r_p$$

Eqn. 7

$$\sigma_r = -2\sigma_\theta = -\frac{2}{3}\sigma_y\left(\frac{r_p}{r}\right)^3 \qquad r > r_p$$

Eqn. 8

where p_B is the pressure inside the inclusion, r_p is the plastic zone radius and r_B is the radius of the inclusion. Since the stresses at the boundary of the plastic zone must be continuous, the plastic zone radius is given by:

$$r_p = r_B \exp\left(-\frac{p_B}{2\sigma_y} - \frac{1}{3}\right)$$

Eqn. 9

In this spherically symmetrical case, all the displacements are radial. Conditions of continuity of displacements and radial stresses at the particle/matrix interface give an expression from which p_B can be evaluated:

$$\frac{6\eta G_A \varepsilon_m}{\sigma_y}\left(1+\frac{p_B}{3B_B\varepsilon_m}-\frac{p_B}{3B_A\varepsilon_m}\right)=\exp\left(-\frac{3p_B}{2\sigma_y}-1\right)$$

Eqn. 10

where :

$$\eta=\frac{(1+\upsilon_A)}{3(1-\upsilon_A)}$$

Eqn. 11

B is the bulk modulus and υ_A is Poisson's ratio for the matrix.

Equation 12 can be solved numerically for p_B and its value substituted in Equations 8 to 11 to give σ_r and r_p. Considering the case of a spherical NbC particle transforming to Nb_2O_5 in an infinite IN718 matrix at 600°C, it was first assumed that there was no mismatch between the NbC particle and the matrix prior to oxidation. Then, the mismatch parameter for complete transformation to Nb_2O_5 was calculated using Eqn. 2 and Eqn. 5. Eqn. 10 was then solved to find p_B, taking the matrix phase 'A' to be IN718 and the particle phase 'B' to be Nb_2O_5. For the IN718 matrix at 600°C, E = 168 GPa [42] and υ 0.276 [43], giving a bulk modulus B_A = 127 GPa. No specific elastic property data for Nb_2O_5 was found in the literature, so an assumption of B_B = 142 GPa and υ_B = 0.21 was used, based on typical data for Al_2O_3 and Fe_2O_3.

APPENDIX B

Scott and Thorpe [31] considered the case of a semi-elliptical crack of length *2c* and depth *a* in a plate of thickness *t*. For the case of pure bending the two main expressions used to calculate the Mode I stress intensity factors at the surface ($\theta = 0$) and at maximum depth ($\theta = \pi/2$) in the present paper are:

$$K_{surface} = \left[\left[M_{f(0)}\left(1-0.3\frac{a}{t}\right)\left(1-\left(\frac{a}{t}\right)^{12}\right)\right]+\left[0.394\cdot E(k)\left(\frac{a}{t}\right)^{12}\sqrt{\frac{c}{a}}\right]\right]\frac{\sigma_b}{E(k)}\sqrt{\pi a} \qquad \text{Eqn. 12}$$

$$K_{depth} = M_{f(\pi/2)}\left[1-1.36\left(\frac{a}{t}\right)\left(\frac{a}{c}\right)^{0.1}\right]\frac{\sigma_b}{E(k)}\sqrt{\pi a} \qquad \text{Eqn. 13}$$

where σ_b is the bending stress. $M_{f(0)}$ and $M_{f(\pi/2)}$ are front face correction factors given by:

$$M_{f(0)} = \left[1.21-0.1\left(\frac{a}{c}\right)+0.1\left(\frac{a}{c}\right)^4\right]\sqrt{\frac{a}{c}} \qquad \text{Eqn. 14}$$

$$M_{f(\pi/2)} = 1.13-0.07\left(\frac{a}{c}\right)^{0.5} \qquad \text{Eqn. 15}$$

E(k) is an approximation of an elliptical integral of the second kind given by:

$$E(k) = \left[1+1.47\left(\frac{a}{c}\right)^{1.64}\right]^{0.5} \qquad \text{Eqn. 16}$$

REFERENCES

[1] J. Lankford & S. J. Hudak (Jr), Int. J. Fatigue 9 (1987) 87

[2] S. Suresh & R. O. Ritchie, International Metals Reviews 29 (1984) 445

[3] K. J. Miller Fatigue Fract. Engng. Mater. Struct. 10 (1987) 92

[4] J. F. Barker, Proc. Superalloy 718 - Metallurgy & Applications 1989, Ed. E. A. Loria, TMS, USA, 1989, p. 269

[5] S. P. Lynch, T. C. Radtke, B. J. Wicks & R. T. Byrnes, Fatigue Fract. Engng. Mater. Struct. 17 (1994) 313

[6] A. Andrieu, R. Molins, H. Ghonem & A. Pineau, Mater. Sci. & Engng. A154 (1992) 21

[7] E. Andrieu, G. Hochstetter, R. Molins & A. Pineau, Proc. 3rd Int. Symp. Superalloys 718, 625, 706 and Various Derivatives, 1994, TMS, Warrendale, PA, USA, 1994, p. 619

[8] H. Ghonem & D. Zheng, Metall. Trans. 23A (1992) 3067

[9] P. Shahinian & K. Sadananda, Trans. ASME J. Engng. Mater. & Tech. 101 (1979) 224

[10] H. Ghonem, T. Nicholas & A. Pineau, Fatigue Fract. Engng. Mater. Struct. 16 (1993) 565

[11] H. Ghonem, T. Nicholas & A. Pineau, Fatigue Fract. Engng. Mater. Struct. 16 (1993) 577

[12] J. P. Pedron & A. Pineau, Mater. Sci. & Engng. 56 (1982) 143

[13] E. Andrieu, R. Cozar & A. Pineau, Proc. Superalloy 718 - Metallurgy & Applications, 1989, TMS, Warrendale PA, USA, 1989, p. 241

[14] L. A. James, Engng. Fract. Mech. 25 (1986)305

[15] M. R. Bache, W. J. Evans & M. C. Hardy, Int. J. Fatigue 21 Supp. (1999) S69

[16] D. Fournier & A. Pineau, Metall. Trans. 8A (1977) 1095

[17] J. C. Healy, L. Grabowski & C. J. Beevers, Int. J. Fatigue 13 (1991) 133

[18] T. Denda, P. L. Bretz & J. K. Tien, Metall. Trans. 23A (1992) 519

[19] G. R. Leverant & M. Gell, Trans. Metall. Soc. of AIME 245 (1969) 1167

[20] J. Reuchet & L. Remy, Mater. Sci. & Engng. 58 (1983) 19

[21] J. Reuchet & L. Remy, Mater. Sci. & Engng. 58 (1983) 33

[22] M. Reger & L. Remy, Mater. Sci. & Engng. A101 (1988) 47

[23] M. Reger & L. Remy, Mater. Sci. & Engng. A101 (1988) 55

[24] G. Sjoberg, N-G. Ingesten & R. G. Carlson, Proc. 2nd Int. Symp. Superalloy 718, 625 & Various Derivatives, 1991, TMS, Warrendale, PA, USA, 1991, p. 603

[25] P. A. S. Reed, F. Hachette, D. Thakar, T. Connolley & M. J. Starink, Proc. 8th Int. Conf. Mechanical Behaviour of Materials (ICM8), Victoria, Canada, May 16-21, 1999, Fleming Printing Ltd. Victoria, BC, Canada, 1999, vol. 1, p. 418

[26] T. Connolley, P. A. S. Reed, & M. J. Starink, Proc. 5th International Charles Parsons Turbine Conference, Cambridge, UK, 3-7 July, 2000, Institute of Materials, London, 2000, p. 982

[27] T. Connolley, M. J. Starink & P. A. S. Reed, Proc. 9th International Symposium on Superalloys, Seven Springs, USA, September 17-21, 2000, TMS, Warrendale, PA, USA, 2000, p. 435

[28] J. Z. Xie Proc. 2nd Int. Symp. Superalloys 718, 625 & Various Derivatives, 1991, TMS, Warrendale, PA, USA, 1991, p. 491

[29] T. Connolley, PhD thesis, University of Southampton, 2001

[30] S. J. Moss, Unpublished data, ALSTOM Power, Whetstone, UK, 1998

[31] P. M. Scott & T. W. Thorpe, Fatigue Engng. Mater. & Struct. 4 (1981) 291

[32] D. A. Fletcher, R. F. McMeeking & D. Parkin, J. Chem. Inf. Comput. Sci. 36 (1996) 746

[33] H. Schafer, R. Gruehn & F. Schulte, Angew. Chem. Internat. Ed. 5 (1966) 40

[34] M. J. Starink, P. Van Mourik & B. M. Korevaar, Metall. Trans. A 24 (1993) 1723

[35] J. K. Lee, Metall. Trans. A 11 (1980) 1837

[36] S. Suresh, Fatigue of Materials, Cambridge University Press, Cambridge, UK, 1991, p. 222

[37] K. Sadananda & A. K. Vasudevan, Short Crack Growth Behavior in: Fatigue and Fracture Mechanics Vol. 27, ASTM STP 1296, ASTM, USA, 1997 p. 301

[38] K. Sadananda & A. K. Vasudevan, Int. J. Fatigue 19 Supp. 1 (1997) S99

[39] K. Sadananda & A. K. Vasudevan, Int. J. Fatigue 19 Supp. 1 (1997) S183

[40] K. Sadananda & A. K. Vasudevan, Proc. Third Engineering Foundation International Conference, Small Fatigue Cracks: Mechanics, Mechanisms & Applications, Oahu, Hawaii, 6-11 December, 1998, Elsevier Science, Oxford, UK, 1999, p. 73

[41] K. J. Miller, Fat. Fract. Engng. Mater. Struct. 16 (1993) 931

[42] S. J. Moss, private communication, ALSTOM Power, Whetstone, UK, 1999

[43] Inco Alloys International Information Booklet, Inconel 718, IAI-19/4M/1994, INCO Alloys International, Fourth Edition, 1985